Environmental Fluid Mechanics (2023) 23:603–620
https://doi.org/10.1007/s10652-023-09921-5

ORIGINAL ARTICLE

KmT, detailing layered mixing governed by internal wave breaking

Hans van Haren[1]

Received: 1 July 2022 / Accepted: 20 March 2023 / Published online: 3 April 2023

Abstract
The kilometer-long sub-surface mooring 'KmT', densely instrumented with 760 high-resolution temperature 'T-'sensors, demonstrates details of turbulent mixing in the vicinity of a large seamount. Away from the internal wave breaking zone above the seafloor, turbulence is observed in two cases. It is found in thin layers along isopycnals providing non-smooth dispersal, as well as induced by internal wave breaking following strongly non-linear interaction as in a hydraulic jump more than 500 m above the local seafloor. Turbulence levels for these cases are relatively low and high, respectively, but always one to two orders of magnitude larger than in the ocean interior far from topography. Both cases imply the importance of underwater topography like a seamount for deep-sea turbulence. The seamount functions as a lens focusing internal waves into a turbulence-generator.

Keywords High-resolution temperature observations · Mount Josephine NE-Atlantic Ocean · Non-smooth isopycnal dispersal · Small-scale Kelvin–Helmholtz instabilities · Interior hydraulic jump by internal waves

1 Introduction

In the vertically stably stratified ocean transport is easier along layers of constant density, isopycnally, than across them, diapycnally. This holds for turbulent transport, which is the dominant form of exchange given the large scales of the ocean resulting in very high Reynolds numbers Re, $10^4 < \mathrm{Re} < 10^6$, nearly everywhere. Laminar flows hardly exist, although the slow water-flow motions tempt to picture the deep-sea as a nearly stagnant pool of water, erroneously. As ocean boundaries are a major source for turbulent mixing, mainly via the breaking of internal waves, extended effects of a deep seamount are addressed in this paper on ocean turbulence mechanisms as revealed via detailed observations from a more than 1 km long mooring 'KmT'.

The general view is that filaments of intruding water along isopycnal layers with distinctly different characteristics than waters above and below can be followed across

✉ Hans van Haren
hans.van.haren@nioz.nl

[1] NIOZ Royal Netherlands Institute for Sea Research, P.O. Box 59, 1790 AB Den Burg, the Netherlands

100 km or more in the open ocean [17] or last for months [9]. This occurs in deep-ocean waters as well as in shallow seas [10]. With the dispersing and eventually disappearing of intrusions, other (conservative) suspended and soluble materials that further characterize different water masses become integrated in the ocean circulation.

Double diffusive fluxes have been suggested as a main driver of, for example, intrusive layering between Mediterranean-outflow waters in their NE-Atlantic Ocean environment [30, 36]. However, as the turbulent mixing associated with the homogenization of stratified waters can be particularly large above sloping topography [2], it has been suggested that isopycnal intrusions there may largely transport mixed waters from the near-bottom 'boundary layers' into the interior of a basin. Such topographically induced intrusions may explain 'nepheloid layers' of sediment that are entrained from sloping seafloors and transported more or less along isopycnals into the interior [5], albeit not necessarily above seafloor slopes that critically match those for internal tidal waves [11]. Largest internal wave breaking has been observed above steep 'super-critical' seafloor slopes (e.g., [40]. The strongly turbulent waters associated with the internal wave breaking are transported periodically into the interior whereby motions in the different near-homogeneous, generally thick layers create vertical current differences (shear) in generally thin well-stratified sheets in between. The shear sets up (secondary) Kelvin–Helmholtz turbulent instabilities 'KHi', as has been demonstrated via detailed numerical modelling [41]. In general, layers associate with weaker stratification than average, the sheets with stronger stratification than average [42]. This is generally a suitable definition for present observations (Fig. 1b). While Woods [42] distinguished "laminar flows" in sheets from "weakly turbulent" layers, all flows here are turbulent with larger-scale turbulent overturning in layers than in sheets, as will be presented below.

In this paper, it is hypothesized that these layers extending from sloping topography must be different from 'water mass intrusions' associated with, e.g., Mediterranean outflow in the Atlantic. This is because above sloping topography highly nonlinearly deformed waves transform into upslope propagating bores that induce thus much turbulent mixing that it is considered [39] to be sufficient to maintain the ocean interior stratified as it governs the transport of heat downwards [20]. Although the sloping topography induces rapid re-stratification, after the turbulent overturning, and to within about a meter from the seafloor [39], the thus effective mixing is expected to also periodically destroy intrusions by homogenizing the near-bottom region for brief moments in a breaking-wave phase [41]. Associated intrusions are thus not hypothesized to exist longer than, e.g., a tidal period.

Internal tide breaking above steep topography enhances turbulent mixing over a range of about 300–400 m above the seafloor according to modeling using typical deep-ocean conditions by Winters [41]. On a (tidal) average basis, the stratification is reduced in that vertical range albeit well away from near-homogeneity, but this does not imply a general monotonic vertical decrease in stratification away from the seamount. Locally enhanced stratification in the interior leads to a local flattening or focusing of internal wave characteristics of energy propagation, like hypothetically sketched in Fig. 1a, rather than the classic large-scale monotonic steepening of characteristics (or wave rays) as previously presented (e.g., [28].

Above hypotheses are investigated in the present observational study that also aims to reveal in some detail the character of intrusions. Additionally, average mixing rates are calculated, the type (shear or convection) of turbulence is determined (using spectral information), and the difference in turbulence between layers near and well-above the

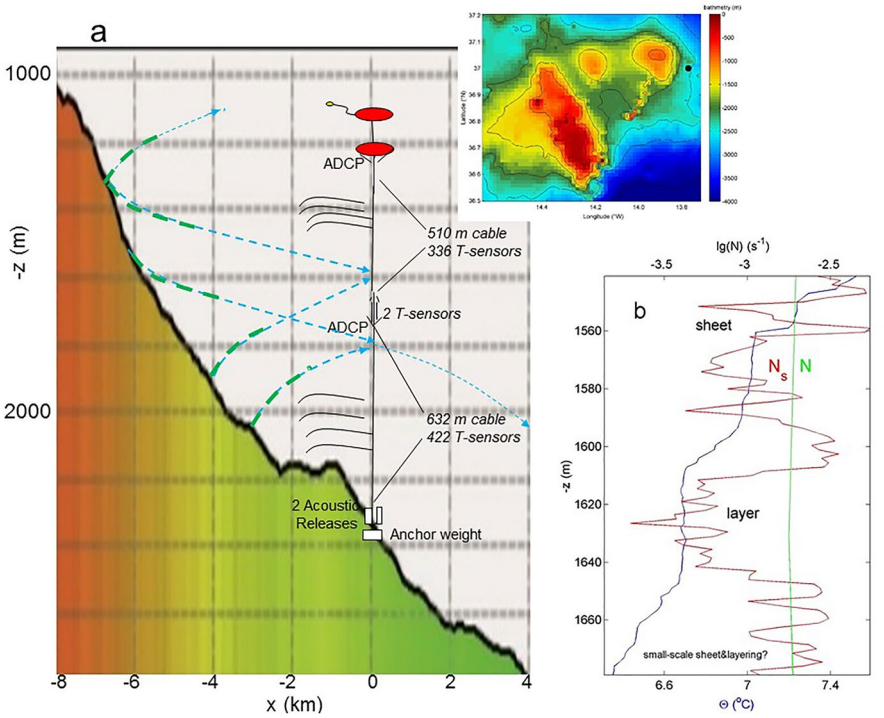

Fig. 1 **a** East–west Multibeam transect along 37°00′N of the bathymetry of Mount Josephine around the mooring site, drawn in an aspect ratio vertical:horizontal = 8:1. The KmT-mooring outline is included, together with schematics of some (of many more possible) semidiurnal internal tide ray-characteristics (indicating the direction of internal wave energy transport; blue-dashed), two groups of equidistant isotherms (thin black lines) and, in green-dashed, of internal-wave breaking spatial extent following a model by Winters [41]. The insert shows the bathymetry from the 1′-version of Smith and Sandwell [32], with the black dot indicating the mooring site. **b** Defining 'sheets' and 'layers' following Woods [42] in a 140-m tall individual profile of temperature data from Fig. 3a. N denotes the 100-m-large scale buoyancy frequency, N_s the 1.5-m-small scale version (logarithmic scale on top)

seafloor are discussed. The detailed observations are inspired by previous observational works like those by Lazier [15], Marmorino et al. [18], Thorpe and White [35], Alford and Pinkel [1].

After a description of materials and methods in Sect. 2, the observations are presented in Sect. 3, and their relevance for turbulent mixing is discussed in Sect. 4.

2 Materials, background conditions and methods

KmT, an 1140 m long thermistor string mooring array, was located at 37° 00′N, 013° 44.5′W, H = 2380 m water depth on an eastern flank of Mount Josephine (Fig. 1), in the NE-Atlantic Ocean about 400 km southwest of Lisbon (Portugal) on 25 April 2019 (yearday 114). It was recovered after four months on 26 August 2019 (yearday 237). The local inertial frequency f = 1.21 cpd, short for cycles per day. During the mooring handling

cruises, shipborne SeaBird-9plus Conductivity-Temperature-Depth (CTD) data were obtained within 1 km from the mooring site.

A total of 760 NIOZ4 high-resolution temperature 'T' sensors [37] were taped to the nylon-coated 0.006-m outer diameter steel cable and to an inline-frame approximately halfway the cable. The 1.50-m vertically separated T-sensors sampled at a rate of once per second. A 4.2-kN elliptic buoy was at 1105 m, 100 m above a similar second buoy holding a downward looking 75-kHz, 20°-slant angle to the vertical RDI/Teledyne acoustic Doppler current profiler 'ADCP'. The inline-frame held a second 75-kHz downward looking ADCP to cover the lower 600-m range of the T-sensors. The ADCPs sampled at a rate of once per 900 s average values in 60 vertical bins of 10 m.

The mooring assembly was held tautly upright with net 5-kN buoyancy and the 8-kN bottom-weight generated net-anchoring with approximately 3 kN. The ADCPs tilt and pressure sensors demonstrated that even under maximum 0.3 m s^{-1} current-flow speeds the top of the mooring deflected little, vertically by < 0.2 m and horizontally by < 20 m. These mooring deflections have negligible effects on the results, as the vertical deflection is well less than half the vertical interval between the T-sensors. No corrections are needed to the T-sensor positioning.

The average local seafloor slope is $\gamma = 9 \pm 1° >> \beta_{M2} = 3.5 \pm 1.5°$ for freely propagating M_2 internal tide characteristics (Fig. 1) under mean local stratification conditions of buoyancy frequency $N = 25 \pm 7$ cpd ($1.8 \pm 0.5 \times 10^{-3}$ $s^{-1} > 10f$). The site is therefore considered supercritical for propagating internal tidal waves. Over the > 1 km vertical range of T-sensors, the wave-slope characteristics vary by a factor of 1.8. CTD-profiles demonstrate a persistent local maximum of N between 1800 and 1350 m and local minima in the lower 200–400 m above the seafloor. Accordingly, the slopes of internal-tide characteristics are sketched, being steep near the seafloor, flatter in the mid-interior, and slowly steepening towards the interior-deep (Fig. 1a).

The top of the mooring occasionally reached into Mediterranean Sea outflow waters, potentially between about 1000 and 1400 m. Hence, partially salinity-compensated apparent density inversions in temperature were registered in the upper range of the measurements at times. Non-turbulence-induced artificial inversions are recognizable in the temperature records as thin-layer instabilities lasting longer than a day. They can be distinguished from genuine turbulent overturning which are not expected to last longer than one inertial period (e.g., [6]. Mediterranean-outflow intrusions are excluded from turbulence analyses.

CTD-data are used to establish the linear temperature-density relationship $\delta\sigma_2 = \alpha\delta\Theta$, $\alpha = -0.053 \pm 0.01$ kg m^{-3} K^{-1} over the entire vertical range of moored T-sensors. Here, Θ denotes Conservative Temperature (IOC, SCOR, IAPSO 2010) and σ_2 the potential density anomaly referenced to a level of 2×10^7 N m^{-2}. Conservative Temperature is dynamically identical to potential temperature, but differs slightly in absolute value. It is the present-day UNESCO-standard and follows from the thermodynamic description of seawater based on a Gibbs function formulation from which thermodynamic properties such as entropy, specific volume, enthalpy and potential enthalpy are calculated directly [13]. Outside moments of upper-layer Mediterranean-outflow intrusions, turbulence parameter values are calculated using the tight temperature-density relationship following the sorting method of Thorpe [34], with constant mean overturning scale and mixing efficiency factors [7, 8, 24, 25], see for more details [39]. Vertically sorted temperature data are used to compute 1.5-m-scale buoyancy frequency N_s that represents 'small-scale stratification', while 100-m-scale N represents 'large-scale stratification' (Fig. 1b). For quantitative purposes, mean values of turbulence dissipation rate ε (m^2 s^{-3}) and eddy diffusivity K_z (m^2 s^{-1} are

calculated by averaging over entire turbulent overturns in the vertical [] or in time < >, or both.

3 Observations

As the observations show a distinct, albeit not-exclusive semidiurnal tidal dominance including the fortnightly spring-neap cycle, the focus will be on evaluation of one representative cycle when Mediterranean outflow effects were undetectable throughout the range of observations. Although Conservative Temperature is presented and used throughout, it will henceforth be referred to in the text as 'temperature' for short.

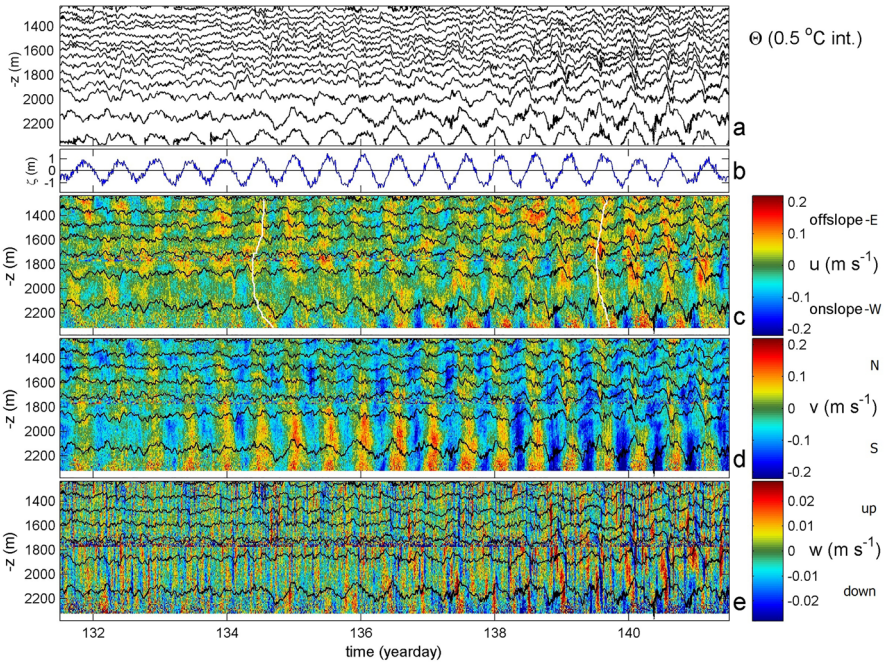

Fig. 2 Ten days, 1140 m overview of moored data from just before a neaps to just after the subsequent springs. **a** Time-depth plot of Conservative Temperature from T-sensor data subsampled at once per 60 s. The seafloor is at the level of the time-axis. Black contours are drawn every 0.5 °C, starting at 3 °C, and the 1 °C-interval ones are repeated in c.-e., for reference. **b** Time series of sea-level excursions relative to their mean value, inferred from 900-s sampled upper ADCP-pressure data. Note the 100-fold larger vertical scale compared to a., c.-e. **c** Window as a., but for East–West horizontal current component from 900-s sampled, 10-m binned ADCP-data. The two white curves are visually drawn co-phase lines. **d** As c., but for North–South horizontal current component. **e** As c., but for vertical current component. The scale is different compared to c., d

3.1 Overview

Above the mid-slopes of Mount Josephine tidal motions are dominant in most physical observables, including temperature isotherm excursions (Fig. 2a), pressure (Fig. 2b), and horizontal current components (Fig. 2c, d). Vertical currents are dominated by high-frequency internal wave motions, of which some are modulated on a tidal periodicity especially near the seafloor (Fig. 2e).

While current and temperature variations are dominated by baroclinic internal tidal waves that provide vertical phase differences over limited vertical ranges of a few 100 m, pressure represents barotropic surface tides mainly. Comparison between the O(1-m) amplitudes of surface excursions (Fig. 2b) with the O(100-m) internal isotherm excursions near the seafloor (Fig. 2a) confirm the dominance of barotropic and baroclinic motions, respectively. The vertical phase difference is manifest between individual isotherms and in cross-slope flow component, with a banana form (Fig. 2c). This form, with upward phase advance from about 1800 m in the upper layer of the T-sensor range and downward phase advance in the lower layer, suggests an energy-focusing for propagating internal waves. This is because the form implies upward energy propagation in the lower layer and downward energy propagation in the upper layer, the focusing being around 1800 m. Such banana form is also visible in modeled cross-slope flows that associate with non-linear internal wave breaking near the top of a seamount [16], but not mentioned in that paper. It is also visible, but not mentioned, in cross-slope flow observations over the deep Oregon shelf as presented in the review-paper by Klymak et al. [14], although not in the original paper [22].

Over time, varying phase differences are observed referencing the surface tide, for example with the lower isotherm. Likewise, spring-neap cycles vary between the different observables. While the surface excursion shows springs around day 137 (Fig. 2b), the isotherms and horizontal current components show springs around day 139. The apparent enhanced positive v-motions are attributable to increased northward flow around day 136. Like the isotherms, the current components show considerable vertical variability, with near-seafloor amplitudes about doubling those 1000-m higher up during springs. Henceforth, neaps will refer to the internal tidal neaps of isotherms and current components, not to the surface tidal neaps. Similar for springs.

3.2 Neaps

In Fig. 3, one inertial period $T_f = 2\pi/f$ of observations during neaps emphasizes the quasi-erratic behavior of internal waves already noted in the 10-day overview of Fig. 2. The vertical axis in Fig. 3a also displays cross-slope horizontal coordinate x using the transform $x = -(z + H)*\sin(\gamma)$. This simply relates isotherm-variations also horizontally besides vertically to the seamount (Fig. 1a), for a different perspective. While also during neaps largest isotherm excursions occur near the seafloor (Fig. 3a), the 1.5-m-scale buoyancy frequency scaled with time-mean values shows a more even distribution in the t,z domain (Fig. 3b). Short-term, high-frequency internal waves dominate the image and demonstrate considerable vertical phase differences (Fig. 3a), like the internal tides in Fig. 2c. The sheets and layers are manifest of internal wave straining, most likely, and show step-like vertical profiles (cf. Figure 1b) which are, however, considerably smoothed on the edges by turbulence activity and only occasionally (infinitesimally) sharp. The sheet&layer

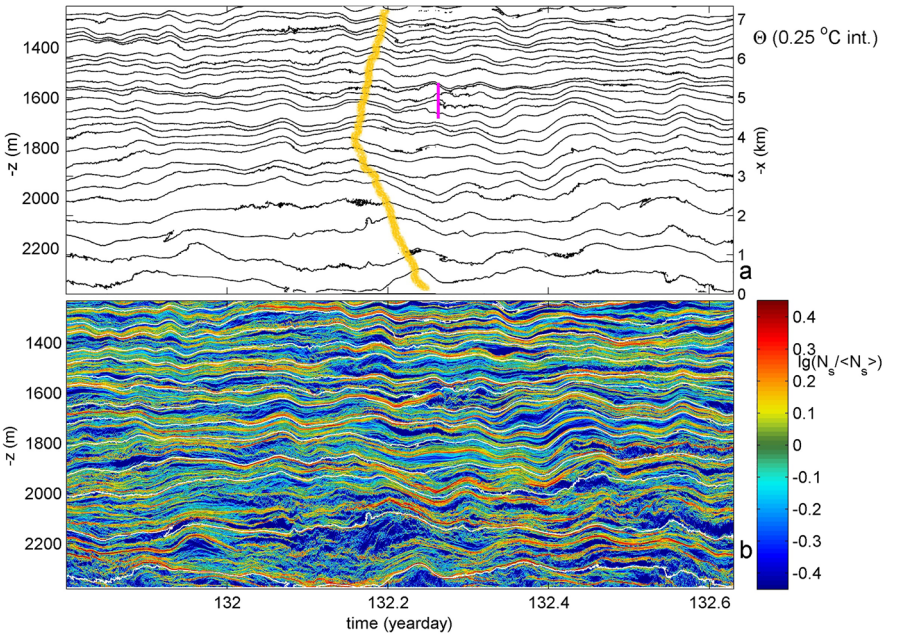

Fig. 3 One-inertial, 1.6-semidiurnal-lunar period (0.83-day) magnification around (thermal) neaps in Fig. 2. In both panels, the seafloor is at the level of the time-axis. **a** Time-vertical plot of Conservative Temperature from T-sensor data sub-sampled at 0.1 Hz, with black contours at 0.25 °C intervals, starting at 3 °C. The vertical axis also displays cross-slope coordinate x, see text (scale to the right). The yellow line is a visually drawn co-phase line interpretation. The small purple line indicates the profile of Fig. 1b. **b** Time-depth plot of logarithm of buoyancy frequency calculated from the vertically sorted version of a. and scaled with its time means at every T-sensor level. The white contours are copies of every other, 0.5 °C-spaced, black contours in a., for reference

thicknesses vary and are regularly of similar size and are only occasionally clearly different in size, like between 1500 and 1600 m.

The smoothing of vertical steps in temperature is a result of regularly occurring turbulence, which is predominantly found in the layers. Evident in the buoyancy frequency image are the short durations of the sheets and layers: None last longer than an inertial period before changing sign (in the scaled image), becoming stronger or weaker than average and vice versa. There is a tendency for sheets to last longer than layers, with some sheets lasting up to about 0.7–0.8T_f and layers (well) less than 0.5T_f. Likewise, isotherms follow sheets and/or layers, but always with shorter duration than an inertial period before changing to another sheet or layer. The associated turbulent mixing is visible in large layers such as around 2200 m and day 132.2, but also in thinner layers higher up (e.g., around 1900 and day 132.5).

Closer inspection in further time-depth magnifications demonstrates the irregular patterns in temperature (Fig. 4) and stratification (Fig. 5) due to turbulent overturning. The overturning primarily affects the stratification in the layers, but the more smoothly internal-wave supporting sheets are also affected by small-scale overturns, disruptions, and deformations. This secondary turbulent overturning is widely distributed in the images and not only sporadically occurring as in the open ocean [38]. This may be a manifestation of the nearby seamount, see modeling results in Klymak et al. [14] and Winters [41], although

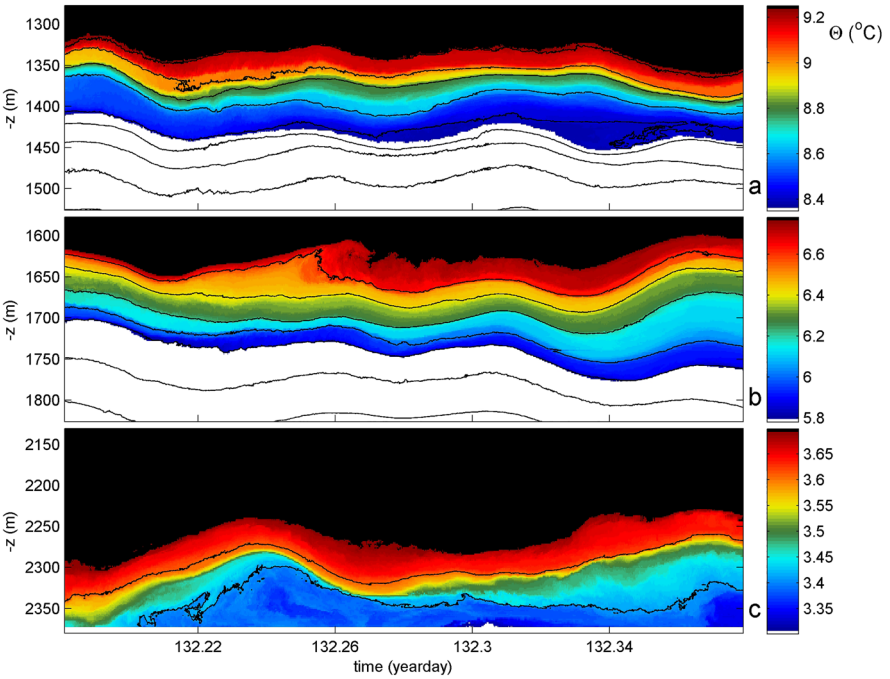

Fig. 4 4.8-h (about one-quarter inertial period) and 250-m magnifications of Fig. 3a for original 1-Hz data, with black contours drawn every 0.2 °C. The colour scales are adapted to highlight particular phenomena in each panel

it is noted that in the upper layers the seamount is more than –x = 5 km away horizontally. The turbulence seems mostly shear-induced, following the form of overturning, and less driven by (buoyancy) convection like the interpretation of plumes in layers in Sargasso Sea observations [18].

Layering of alternating stronger and weaker stratified waters is moved up and down by high-frequency internal waves (Figs. 3, 4 and 5). Despite the layering and the overall stable stratification in density, turbulent activity is regularly visible. This activity varies from spectacular wave breaking in the interior, such as between 1600 and 1650 m around day 132.26 (Fig. 4b), note this is not a small breaker of several 10's of meters height, but also in more elongated form around 1750 m lasting nearly 3 h with varying intensity between days 132.19 and 132.3 (Fig. 5b). This long duration exceeds the mean large-scale buoyancy period of about 1 h (which obviously associates with the dominant internal wave period visible), but is smaller (by a factor of 0.9) than the local buoyancy period in the weakly stratified layer. Notable are the small cusps of < 15 min duration that border the weakly stratified layer. These cusps delineate the individual overturns, which are thus of much shorter duration than the mean buoyancy period, but also shorter than the minimum small-scale buoyancy period of 1110 s in the record (as determined from the maximum $N_{s,max}$ of the 1.5-m-small-scale buoyancy frequency data.)

Thin-layer stratification, sometimes being just one pixel thick, varies largely along with isotherms, but the reader is invited to follow a particular isotherm with time and find out that departures between thin-layer and isotherm occur regularly and seemingly

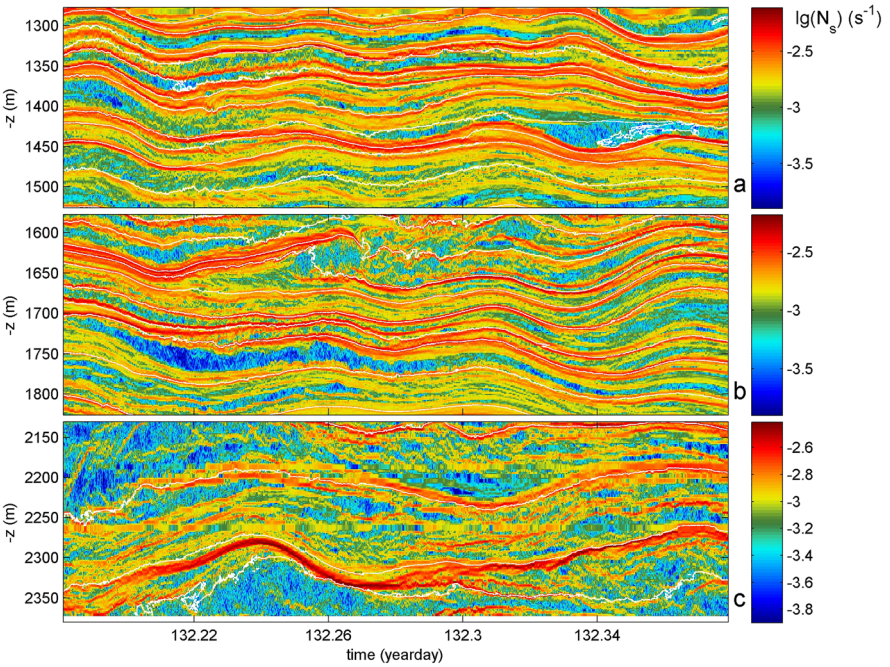

Fig. 5 As Fig. 4, but for the logarithm of buoyancy frequency and with white isothermal contours. The colour scales are adapted to accommodate for the vertical variation in mean buoyancy frequency, which decreases with increasing depth

unexpectedly (Fig. 5). Such departures are associated with wave breaking, see around the larger breakers, and take up their previous distancing after one local buoyancy period. See for instance the upper three isotherms in Fig. 5b and their large breaker in between. None of the observed turbulence is associated with artificial intrusions, and represents genuine turbulent overturns. It is unclear whether the observed activity in this depth-range has an association with wave breaking at the seamount of which the seafloor is several km away horizontally. Or, the breaking is generated locally induced by the non-linear interactions. What induces the sweep-up of the internal wave amplitude on day 132.35 is also unclear. Locally, these internal waves are almost phase-consistent, local mode-1 waves, whereas the smaller waves before showed large vertical phase differences. Analysis from the data of Figs. 4c and 5c provides 0.2-d and 240-m mean value of $[<\varepsilon>] = 1.0 \pm 0.6 \times 10^{-8}$ m^{2}s^{-3}, for identical $N \equiv [<N_s>] = 1.9 \pm 0.2 \times 10^{-3}$ s^{-1}.

3.3 Springs

While turbulence is manifest during neaps throughout the range of observations, it is more intense during springs, not only near the seafloor (Figs. 6, 7 and 8). Sheets and layers become more deformed, although sheets still last longer than layers. As during neaps, layers are larger near the seafloor than higher-up in the range. A notable event occurs around z = -1700 m on day 139.58: A 100-m tall hydraulic jump is observed relatively far from topography as the sloping seafloor is at least 600 m away vertically and 4 km

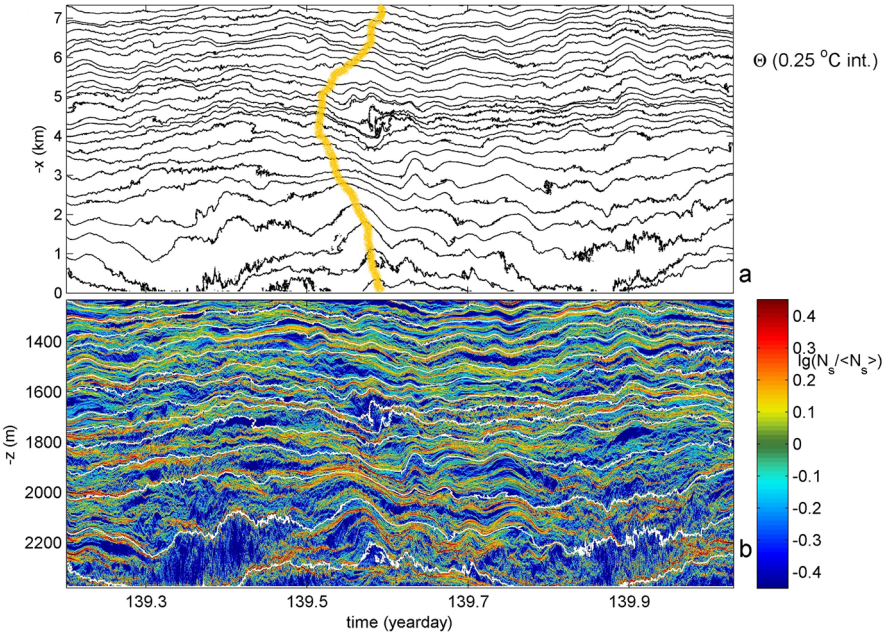

Fig. 6 As Fig. 3, but for springs. In a., only the *x*-coordinate is given

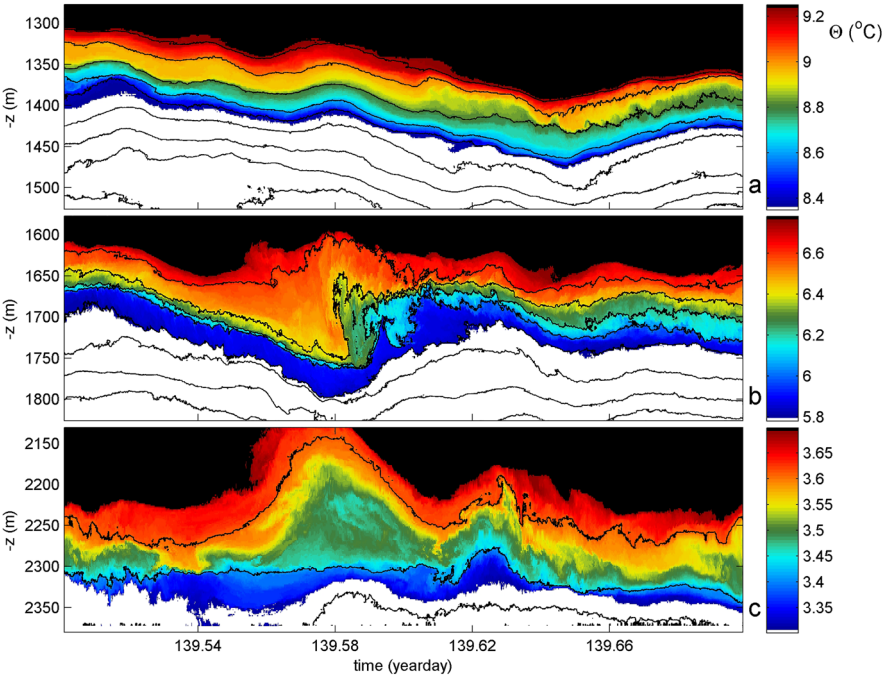

Fig. 7 As Fig. 4, but for springs

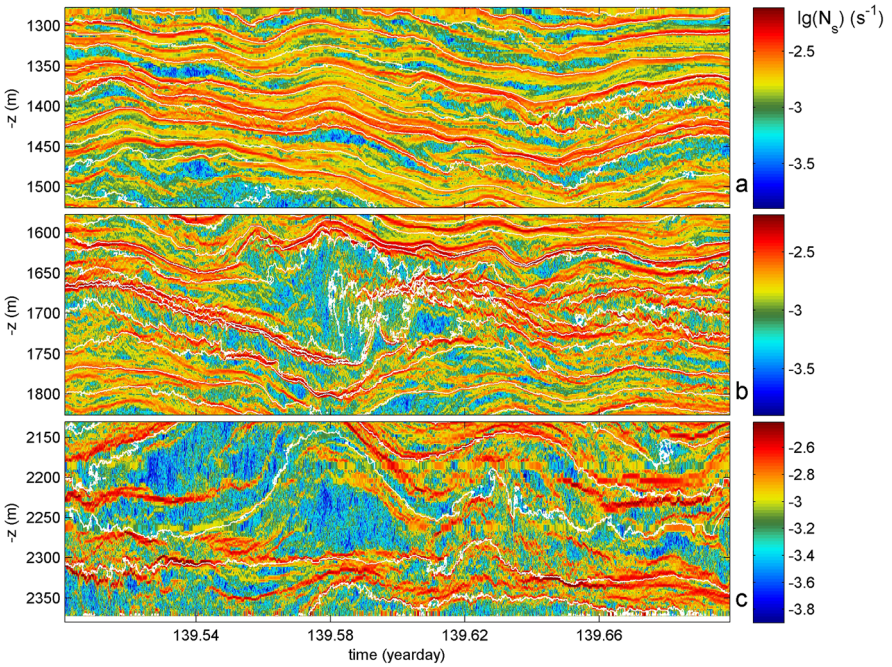

Fig. 8 As Fig. 5, but for springs

horizontally. Although somewhat arbitrary also because of the rather coarse water-flow sampling by ADCP, the lee-wave Froude number [19] $Fr_l = Nh/U \approx 1.4$ for flow-amplitude $U = 0.15$ m s^{-1}, $N = 2.1 \times 10^{-3}$ s^{-1} and scale-height $h = 100$ m.

The jump and subsequent 100-m interior overturn associate with the time of passage of the crest of the internal tidal wave near the seafloor, of which the downward phase propagation started around 1700 m just before the jump's initial occurrence. As above the jump the phase propagation seems upward, the associated downward (upper layer) and upward (lower layer) energy directions for freely propagating internal waves seem to focus near the level of the hydraulic jump. The jump thus seems retarded by the local internal wave energy focusing during springs before being sufficiently non-linear to overturn upon release. Such large interior hydraulic jump has been observed during three semidiurnal periods around the time of springs. The time and location of occurrence of the hydraulic jump contrast with previously modeled and observed hydraulic jumps near the crest of underwater topography and which occur at the turn of the tide associating with an upslope propagating bore (e.g., [16]. Here, it associates with off-slope flow at the start of the downward warming phase of the tide and it is found in the ocean interior well above topography. The internal wave focusing is the indirect effect of the seamount potentially inducing the interior hydraulic jumps.

Not only a spectacular 100-m tall overturn is observed around 1700 m of which the core lasts about 2700 s (a factor of 0.9 times the local mean buoyancy period), but almost the entire image is filled with turbulent overturning above noise level (Figs. 7 and 8). About 1 h after the strong mixing of the hydraulic jump, isotherms above its core show large variability (1650 m, 139.63). For Figs. 7b and 8b, the 0.2-d and 240-m mean $[<\varepsilon>] = 1.2 \pm 0.7 \times 10^{-7}$ m^{2}s^{-3}, for $N \equiv [<N_s>] = 2.1 \pm 0.2 \times 10^{-3}$ s^{-1}. This

turbulence dissipation rate value is of the order of magnitude of that found in turbulent bores propagating up the sloping seafloor. It is noted that the 2-h internal wave in the lower layer also shows comparable turbulent overturning, which, however, barely reaches the seafloor and is not expected to contribute much to sediment resuspension (Figs. 7c and 8c). It is unclear whether increased activity in the upper layer after day 139.59 in Figs. 7a and 8a is associated with the large turbulent overturning in the layers below. Evident are small, 10–20-m, scale KHi.

3.4 Overview (2)

The interior overturning during springs is manifest in the vertical profiles of time-averaged turbulence values (Fig. 9). In the method proposed by Thorpe [34] individual displacements of unstable density have little meaning and only values averaged over entire turbulent overturns, either in z or in t as employed here, are used for quantification. The effect of a large overturn on averages over quarter-inertial-period values is more evident in the interior than near the seafloor, whilst it is smaller on the averages over one inertial period. In general, springs turbulence values are larger by less than half an order of magnitude compared to neaps. Largest values are observed near the seafloor, where stratification is weaker than higher up, albeit by less than a factor of two in buoyancy frequency. In the

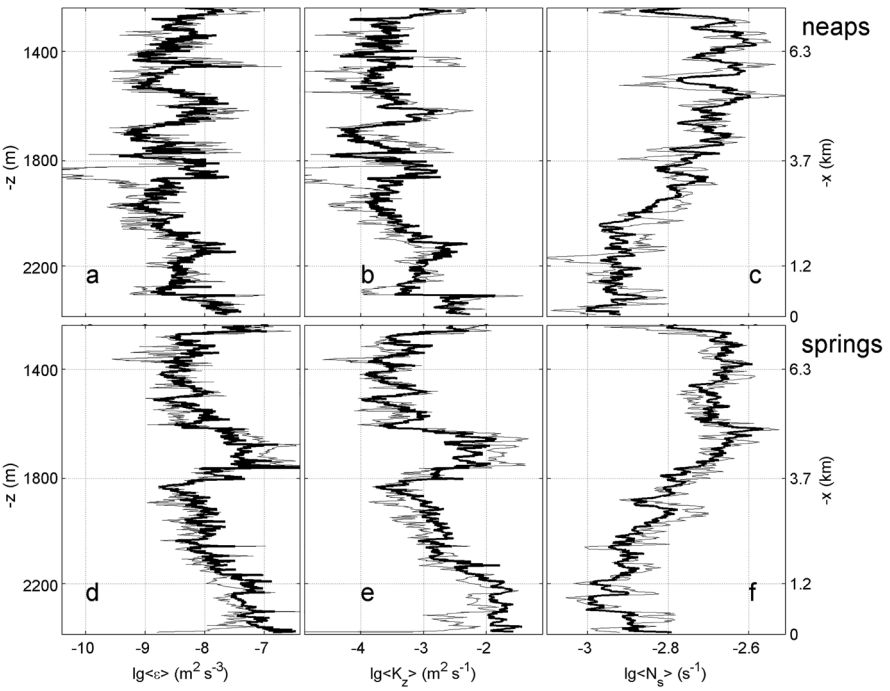

Fig. 9 Profiles of time-mean values of turbulence parameters for data in Figs. 3–5 (neaps: a.-c.) and Figs. 6–8 (springs: d.-f.). In all panels the thick lines represent the one-inertial-period means of Figs. 3,6, and the thin lines the quarter-inertial-period means of Figs. 4,5,7,8. **a** Logarithm of turbulence dissipation rate during neaps. **b** Logarithm of eddy diffusivity during neaps. **c** Logarithm of buoyancy frequency during neaps. **d** As a., but during springs. **e** As b., but during springs. **f** As c., but during springs

upper range, buoyancy frequency also decreases confirming the persistency of a local buoyancy frequency maximum vertically between about 1300 and 1800 m. Apart from the large overturn around mid-range during springs, time-mean turbulence values are organized in vertical layers of 100–200 m. This layering is approximately equivalent to the layer of largest turbulence values near the seafloor, and may reflect the interior isopycnal transport of the waters mixed just above the sloping seafloor by internal wave breaking at any position along the steep seafloor slope. Previous observations from a nearby site above steep slope of the same seamount confirm ample similar turbulent mixing [40]. If transported from the seamount floor, the intruding layers need to propagate several kilometers horizontally from the slope. Such mechanism has to compete with local internal-wave straining, noting that such waves may result from (breaking) interaction at the seamount.

The turbulence intensities, even at more than 5 km horizontally away from the seamount, demonstrate that the mixing at the seafloor by breaking internal waves is not smoothly transported along isopycnals into the interior, but vigorously turbulent. This confirms modeling by Winters [41], but for the first 1–2 km from the slope only. Although the time-mean values vary over two orders of magnitude, the vertical decrease over the

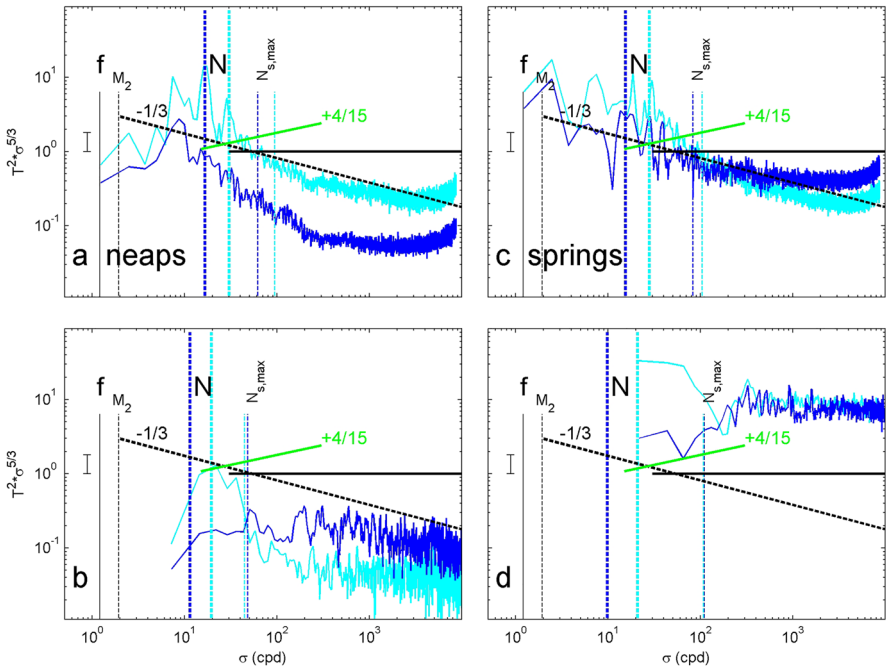

Fig. 10 Mean spectra for upper (1450–1600 m; light-blue) and lower (2170–2320 m; blue) layers. Left column shows data during neaps, right column data during springs. All spectra are scaled with the inertial subrange slope -5/3 (horizontal black line) and considerably smoothed (350 degrees of freedom). Vertical lines indicate inertial frequency f, local mean and maximum buoyancy frequencies N and $N_{s,max}$, respectively, and semidiurnal lunar tidal frequency M_2. Sloping lines are explained in the text. **a** Log–log plot of temperature variance from 0.2-Hz subsampled data in Fig. 3a **b** As a., but for 1.25-h, 1-Hz sampled subsets in Fig. 4a,c. **c** As a., but for data from Fig. 6. All slopes are identical as in a., for reference, but vertical lines show locally calculated values (except for M_2). **d** As b., but for data from Fig. 8b and, for reference, from Fig. 11a (days $139.32 < t < 139.37$, $-2372 < z < -2222$ m)

entire 1140-m range of smoothed profiles is about one order of magnitude in the lower half only, being constant in magnitude in the upper half.

As a result, temperature variance spectra between the upper and lower layers differ in internal wave and turbulence content, but not greatly (Fig. 10). In Fig. 10, the frequency (σ) spectra of 150-m vertically averaged data are scaled with $\sigma^{-5/3}$, the spectral slope of the inertial subrange of turbulence induced by shear [33]. Convection turbulence has a slope of $\sigma^{-7/5}$ and renders a slope of +4/15 in an inertial-subrange-scaled log–log plot [4, 26]. During the inertial period of neaps, the spectra slope steeper than σ^{-2} for $\sigma > N$, and slightly steeper in the lower layer (Fig. 10a). Such slopes at super-buoyancy frequencies might indicate dominant finestructure contamination [27, 29] because they cannot represent freely propagating internal waves, but small spectral slope changes do not confirm this.

At a certain $\sigma > N$, the lower-layer spectrum rather abruptly changes to a slope of $\sigma^{-5/3}$ at about 200 cpd and remains at this turbulence inertial subrange characteristic up to divergence to white noise. This change to the inertial subrange is also seen in the upper-layer data, but remains so only for a limited frequency band between [200, 400] cpd before rolling off further at a rate of σ^{-2}.

The existence of a (dominant) inertial subrange at high frequencies supports the evidence of relatively large turbulence values in the layers, also during neaps. During brief moments of time and exclusively sampling in layers for 1.25 h demonstrates extended inertial subranges, also in the upper layer (Fig. 10b). In that example, the lower-layer inertial subrange extends between N and 6000 cpd (roll-off frequency), with possibly (insignificant) indication of a convective subrange between N and 200 cpd. Convection turbulence does not appear dominant in these data. The upper-layer inertial subrange commences at about 100 cpd after roll-off from a peak between N and $N_{s,max}$.

During springs, the tidal variance increases as well as the high-frequency inertial subrange levels of the lower layer (Fig. 10c). In contrast, the upper-layer band between about N and 5000 cpd remains almost identically the same as during neaps. Like during neaps, no indication is found for finestructure contamination. This may be because turbulence levels are too high, especially during short periods in particular layers (Fig. 10d). During these short springs periods, the inertial subrange extends in both layers between about 100 and 5000 cpd before rolling off, reflecting dominant shear-induced turbulence as during neaps. Following the model by Winters [41], the dominant shear is likely induced by secondary KHi, that are reflected in the rugged upper and lower edges in layers observed here.

Only during the first hour after a frontal bore passage just above the seafloor, a significant convective subrange slope is observed, as shown in the reference-spectrum of Fig. 10d. That spectrum shows considerable temperature variance in the inertial subrange but small variance at N. The large turbulence between days 139.32 and 139.37 in the lower 150 m above the seafloor is associated with low Fr_l-values < 0.25 but also low gradient Richardson number $Ri = N^2/S^2 < 0.25$ (Fig. 11). Note that 10-m Ri-values are computed for near-inertial shear as these were the only to exceed ADCP-instrumental noise levels. While 'critical' Froude numbers, which distinguish flow passing an obstacle like topography from blocking and splitting, vary between $Fr_l = 1.0$ for one-dimensional (1D)-flow, 0.7 for 2D-flow and 0.4 for 3D-flow [23], the turbulent bore itself shows generally lower values for a scale-height of 100 m. As the overturns grow larger up to nearly 200 m, perhaps h = 200 m is a better scale for such bores, which doubles the Fr_l-values for this case. While $Ri < 1$ are found for $z < -2200$ m around day 139.4, $Fr_l < 0.4$ extend up to $z < -2050$ m and $Fr_l < 0.7$ up to $z < -1900$ m.

The low Froude numbers, and the low Ri-values although over a smaller t,z-range, are found to coincide with the zone of high turbulence dissipation rate values. This contrasts with the observations around the internal hydraulic jump detailed in Fig. 7b, which shows (for

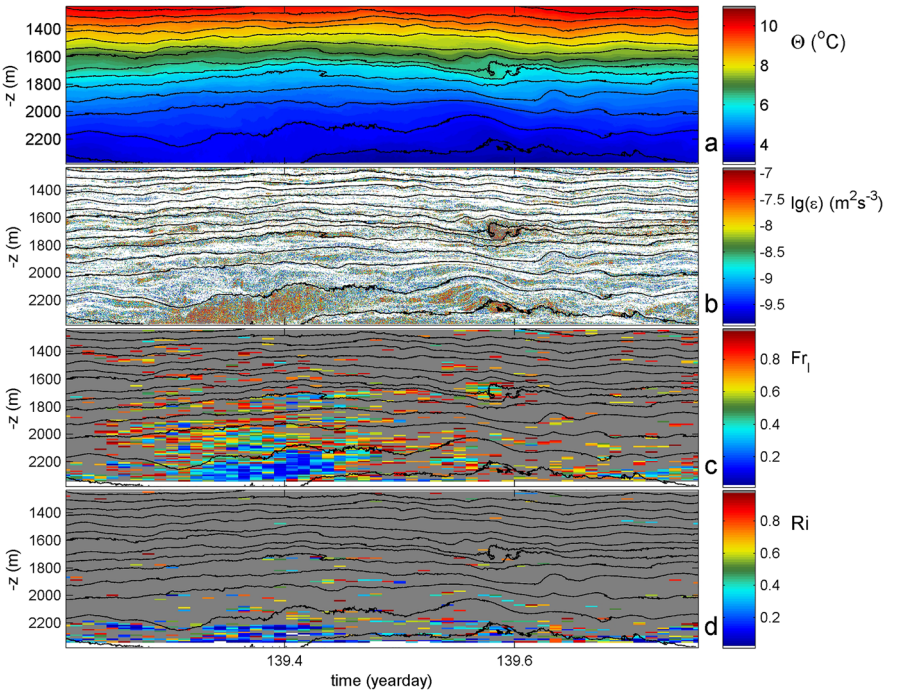

Fig. 11 Flow character of one tidal period during springs in time-depth plots with the horizontal axes at the level of the seafloor. Temperature contours are drawn in black every 0.5 °C. **a** Conservative Temperature. **b** Non-averaged turbulence dissipation rate computed from data in a. **c** Lee-wave Froude number computed from ADCP-data and data in a. sub-sampled to once per 900 s, using a fixed scale-height of 100 m. **d** Gradient Richardson number computed from near-inertial band-pass-filtered ADCP-data and data in a. sub-sampled to once per 900 s and averaged over 10-m vertical intervals

h = 100 m) Fr_l-values between 0.4 and 0.8 but starting about 0.5 h before the most intense turbulence in Fig. 11.

4 Discussion

The present observations show that above a seamount slope layers and sheets are relatively short-lived. They have durations of maximum half a pendulum day, more typical a few hours or once-twice the large-scale mean buoyancy period. For a mean (3-h maximum) U = 0.08 (0.16) m s^{-1} this roughly translates to maximum horizontal extents of 3 (2) km, and more typically 1 km. As these durations are equivalent to observations in the near-surface layer and in the vicinity of slopes (e.g., [1, 6, 12], but much shorter than the weeks-months lifetime of intrusions in the open ocean (e.g., [9, 31], nearby boundary effects are expected to be important for the apparent rapid dispersal of intrusions. This suggests that the stronger turbulence above topography compared with the open ocean, on average by a factor of 100 in a tide-dominated area [39], reduces the life-time of intrusions to a day or less.

The sheet&layering may appear differently throughout the more than 1-km vertical range of observations. However, the applied scaling with local mean buoyancy frequency demonstrates that all sheet&layering is more or less similar, and similarly turbulent, throughout the observations. The similarity is independent of the phase in the spring-neap period.

Most eye-catching effect of the seamount is the generation of internal hydraulic jumps far above local topography and presumably triggered via internal wave breaking at the seafloor. They were not detected in previous smaller and/or less-instrumented moorings. The seamount seemingly functions as a lens for internal wave ray-characteristics emanating from different spots along its sloping seafloor. Thus, Fig. 1 should be modified to reflect this hypothetical mechanism, occurring between 1600 and 1800 m at the present site. Although some previous models and observations showed signs of such interior hydraulic jumps, future modelling may provide details on the suggested mechanism. This could reveal further aspects of the importance of underwater topography for maintenance of the ocean stratification, paradoxically via sufficient turbulence generation, for transporting heat downward and preventing a stagnant pool of cold water to maintain viable deep-sea life [21]. It seems that the effects of topography-induced mixing reach further into the ocean than previously thought, although differently than sketched in [3].

Acknowledgements I thank captain and crew of R/V Pelagia for their assistance and technicians of NIOZ-NMF for help in preparing and deploying the mooring. NIOZ-temperature sensors have been funded in part by the Netherlands Organization for the Advancement of Science (N.W.O.).

Funding Aard- en Levenswetenschappen, Nederlandse Organisatie voor Wetenschappelijk Onderzoek.

Data availability Data will be made available on reasonable request.

Declarations

Conflict of interest H.V.H. declares no conflict of interest.

References

1. Alford MH, Pinkel R (2000) Overturning in the thermocline: the context of ocean mixing. J Phys Oceanogr 30:805–832
2. Armi L (1978) Some evidence for boundary mixing in the deep ocean. J Geophys Res 83:1971–1979
3. Armi L (1979) Effects of variations in eddy diffusivity on property distributions in the oceans. J Mar Res 37:515–530
4. Bolgiano R (1959) Turbulent spectra in a stably stratified atmosphere. J Geophys Res 64:2226–2229
5. Cacchione DA, Drake DE (1986) Nepheloid layers and internal waves over continental shelves and slopes. Geo-Mar Lett 16:147–152
6. Dale AC, Levine MD, Barth JA, Austin JA (2006) A dye tracer reveals cross-shelf dispersion and interleaving on the Oregon shelf. Geophys Res Lett 33:L03604. https://doi.org/10.1029/2005GL024959
7. Dillon TM (1982) Vertical overturns: a comparison of Thorpe and Ozmidov length scales. J Geophys Res 87:9601–9613
8. Gregg MC, D'Asaro EA, Riley JJ, Kunze E (2018) Mixing efficiency in the ocean. Ann Rev Mar Sci 10:443–473
9. Hebert D, Oakey N, Ruddick B (1990) Evolution of a mediterranean salt lens: scalar properties. J Phys Oceanogr 20:1468–1483

10. Holtermann PL, Prien R, Naumann M, Mohrholz V, Umlauf L (2017) Deepwater dynamics and mixing processes during a major inflow event in the central Baltic Sea. J Geophys Res 122:6648–6667. https://doi.org/10.1002/2017JC013050
11. Hosegood P, van Haren H (2004) Near-bed solibores over the continental slope in the Faeroe-Shetland Channel. Deep-Sea Res II 51:2943–2971
12. Inall ME (2009) Internal wave induced dispersion and mixing on a sloping boundary. Geophys Res Lett 36:L05604. https://doi.org/10.1029/2008GL036849
13. IOC, SCOR, IAPSO (2010) The international thermodynamic equation of seawater – 2010: Calculation and use of thermodynamic properties. Intergovernmental Oceanographic Commission, Manuals and Guides No. 56, UNESCO
14. Klymak JM, Legg S, Alford MH, Buijsman M, Pinkel R, Nash JD (2012) The direct breaking of internal waves at steep topography. Oceanography 25:150–159
15. Lazier JRN (1973) Temporal changes in some fresh water temperature structures. J Phys Oceanogr 3:226–229
16. Legg S, Klymak J (2008) Internal hydraulic jumps and overturning generated by tidal flow over a tall steep ridge. J Phys Oceanogr 38:1949–1964
17. May BD, Kelley DE (2001) Growth and steady state stages of thermohaline intrusions in the Arctic Ocean. J Geophys Res 106:16783–16794
18. Marmorino GO, Brown WK, Morris WD (1987) Two-dimensional temperature structure in the C-SALT thermohaline staircase. Deep-Sea Res 34:1667–1676
19. Mayer FT, Fringer OB (2017) An unambiguous definition of the Froude number for lee waves in the deep ocean. J Fluid Mech 831:R3
20. Munk WH (1966) Abyssal recipes. Deep-Sea Res 13:707–730
21. Munk W, Wunsch C (1998) Abyssal recipes II: energy of tidal and wind mixing. Deep-Sea Res I 45:1977–2010
22. Nash JD, Alford MH, Kunze E, Martini K, Kelly S (2007) Hotspots of deep ocean mixing on the Oregon. Geophys Res Lett 34:L01605. https://doi.org/10.1029/2006GL028170
23. Nikurashin M, Ferrari R, Grisouard N, Polzin K (2014) The impact of finite-amplitude bottom topography on internal wave generation in the Southern Ocean. J Phys Oceanogr 44:2938–2950
24. Oakey NS (1982) Determination of the rate of dissipation of turbulent energy from simultaneous temperature and velocity shear microstructure measurements. J Phys Oceanogr 12:256–271
25. Osborn TR (1980) Estimates of the local rate of vertical diffusion from dissipation measurements. J Phys Oceanogr 10:83–89
26. Pawar SS, Arakeri JH (2016) Kinetic energy and scalar spectra in high Rayleigh number axially homogeneous buoyancy driven turbulence. Phys Fluids 28:065103
27. Phillips OM (1971) On spectra measured in an undulating layered medium. J Phys Oceanogr 1:1–6
28. Pingree RD, New AL (1991) Abyssal penetration and bottom reflection of internal tide energy in the Bay of Biscay. J Phys Oceanogr 21:28–39
29. Reid RO (1971) A special case of Phillips' general theory of sampling statistics for a layered medium. J Phys Oceanogr 1:61–62
30. Ruddick B (1984) The life of a thermohaline intrusion. J Mar Res 42:831–852
31. Schmitt RW (1987) The Caribbean sheets and layers transects (C-SALT) program. Eos 68:57–60
32. Smith WHF, Sandwell DT (1997) Global seafloor topography from satellite altimetry and ship depth soundings. Science 277:1957–1962
33. Tennekes H, Lumley JL (1972) A first course in turbulence. The MIT Press
34. Thorpe SA (1977) Turbulence and mixing in a Scottish loch. Phil Trans Roy Soc Lond A 286:125–181
35. Thorpe SA, White M (1988) A deep intermediate nepheloid layer. Deep-Sea Res 35:1665–1671
36. Turner JS (1979) Buoyancy effects in fluids. Cambridge University Press, Cambridge
37. van Haren H (2018) Philosophy and application of high-resolution temperature sensors for stratified waters. Sensors 18:3184. https://doi.org/10.3390/s18103184
38. van Haren H (2019) Open-ocean interior moored sensor turbulence estimates, below a Meddy. Deep-Sea Res I 144:75–84
39. van Haren H, Gostiaux L (2012) Detailed internal wave mixing observed above a deep-ocean slope. J Mar Res 70:173–197
40. van Haren H, Cimatoribus AA, Gostiaux L (2015) Where large deep-ocean waves break. Geophys Res Lett 42:2351–2357. https://doi.org/10.1002/2015GL063329
41. Winters KB (2015) Tidally driven mixing and dissipation in the stratified boundary layer above steep submarine topography. Geophys Res Lett 42:7123–7130. https://doi.org/10.1002/2015GL064676
42. Woods JD (1968) Wave-induced shear instability in the summer thermocline. J Fluid Mech 32:791–800